AIP | Journal of Applied Physics

Electronic band structure and effective mass parameters of Ge1-xSnx alloys

Kain Lu Low, Yue Yang, Genquan Han, Weijun Fan, and Yee-Chia Yeo

Citation: J. Appl. Phys. **112**, 103715 (2012); doi: 10.1063/1.4767381
View online: http://dx.doi.org/10.1063/1.4767381
View Table of Contents: http://jap.aip.org/resource/1/JAPIAU/v112/i10
Published by the American Institute of Physics.

Electronic band structure and effective mass parameters of $Ge_{1-x}Sn_x$ alloys

Kain Lu Low,[1] Yue Yang,[1] Genquan Han,[1] Weijun Fan,[2] and Yee-Chia Yeo[1,a)]
[1]*Department of Electrical and Computer Engineering, National University of Singapore, Singapore 119260*
[2]*Department of Electrical and Electronic Engineering, Nanyang Technological University, Singapore 639798*

(Received 31 July 2012; accepted 26 October 2012; published online 28 November 2012)

This work investigates the electronic band structures of bulk $Ge_{1-x}Sn_x$ alloys using the empirical pseudopotential method (EPM) for Sn composition x varying from 0 to 0.2. The adjustable form factors of EPM were tuned in order to reproduce the band features that agree well with the reported experimental data. Based on the adjusted pseudopotential form factors, the band structures of $Ge_{1-x}Sn_x$ alloys were calculated along high symmetry lines in the Brillouin zone. The effective masses at the band edges were extracted by using a parabolic line fit. The bowing parameters of hole and electron effective masses were then derived by fitting the effective mass at different Sn compositions by a quadratic polynomial. The hole and electron effective mass were examined for bulk $Ge_{1-x}Sn_x$ alloys along specific directions or orientations on various crystal planes. In addition, employing the effective-mass Hamiltonian for diamond semiconductor, band edge dispersion at the Γ-point calculated by 8-band k.p. method was fitted to that obtained from EPM approach. The Luttinger-like parameters were also derived for $Ge_{1-x}Sn_x$ alloys. They were obtained by adjusting the effective-mass parameters of k.p method to fit the k.p band structure to that of the EPM. These effective masses and derived Luttinger parameters are useful for the design of optical and electronic devices based on $Ge_{1-x}Sn_x$ alloys. © *2012 American Institute of Physics*.
[http://dx.doi.org/10.1063/1.4767381]

I. INTRODUCTION

Semiconductor alloys have been extensively used for engineering material properties through tuning the alloy composition. The Si/Ge material system of group IV has been widely studied for applications in optoelectronics and electronics. However, the indirect nature of the band gap of the Si/Ge material system is a fundamental limitation for its application in optoelectronics. $Ge_{1-x}Sn_x$ alloy has emerged as a promising alternative alloy to achieve tunable direct band gaps in group IV diamond-cubic materials. By tuning the Sn composition, the band gap of $Ge_{1-x}Sn_x$ alloys exhibits a transition from indirect to direct. The tunable direct band gap of $Ge_{1-x}Sn_x$ makes possible the fabrication of optical and electronic devices with group IV materials using a complementary metal-oxide-semiconductor (CMOS) compatible process flow.

First-principles and empirical methods have been used for the calculations of $Ge_{1-x}Sn_x$ alloys physical parameters. From first-principles calculations, the optical band gap bowing parameter, b, is reported to be 2.06,[1] 2.75,[2] 2.49,[3] and 1.90,[4] while calculations based on virtual crystal approximation (VCA) generally give a smaller optical band gap bowing (0.94,[5] 0.25,[6] −0.4,[7] and 0.30.[8])

The GeSn material system can be grown epitaxially using various growth techniques such as molecular beam epitaxy (MBE)[9–21] and chemical vapor deposition (CVD).[22–27] Pulsed UV laser annealing of amorphous Ge-Sn film has been used to synthesize the metastable crystalline $Ge_{1-x}Sn_x$ alloys.[28] Other techniques used to grow crystalline $Ge_{1-x}Sn_x$ are dc-diode sputtering[29] and RF sputtering.[30–32] An optical absorption measurement for diamond cubic $Ge_{1-x}Sn_x$ alloys performed by He *et al.*[15] has shown that the range of direct energy gap of $Ge_{1-x}Sn_x$ to be between 0.35 and 0.80 eV for $0 < x < 0.15$. Later, Guevara *et al.*[32] reported that the critical Sn composition x_c corresponding to the transition from indirect to direct band gap is experimentally observed to lie between $0.10 < x_c < 0.13$ determined from transmittance measurements using a fast-Fourier-transform infrared interferometer. Costa *et al.*[27] and Chen *et al.*[20] reported the critical concentration to be 0.11 and 0.071, respectively.

Apart from the band gap energies, the effective masses are important fundamental parameters used in the design of electronic and optical devices. Most of the studies of $Ge_{1-x}Sn_x$ alloys have focused on band gaps and critical composition. However, there is a lack of investigation on the effective mass parameters of $Ge_{1-x}Sn_x$ alloys. Effective mass parameters of $Ge_{1-x}Sn_x$ alloys may be useful for the design of $Ge_{1-x}Sn_x$ alloys-based devices.

First principles calculations generally underestimate the band gap energies and require substantial computational time. The issue of band gap underestimation also becomes worse for narrow band gap materials, such as GeSn system. In this study, the empirical pseudopotential method (EPM) was adopted for calculating the band structures of bulk $Ge_{1-x}Sn_x$ alloys along high symmetry lines in the Brillouin zone for Sn composition varying from 5% to 20%, and the electron and hole effective masses are extracted along various directions on common crystal planes. Based on the band gap energies at L-point and Γ-point obtained from fitting the experimental data,[27] the adjustable parameters of EPM were tuned in order to reproduce the band features that agree with the experimental data.

a)Author to whom correspondence should be addressed. Electronic mail: yeo@ieee.org. Telephone: +65 6516-2298. Fax: +65 6779-1103.

This paper is organized as follows. A brief theoretical background of EPM and the results of $Ge_{1-x}Sn_x$ band structures calculations and effective masses are described in Sec. II. In Sec. III, we review the 8-band k.p model and the derivation of the Luttinger parameters for $Ge_{1-x}Sn_x$ at different Sn compositions. Section IV summarizes the key points of this work.

II. ELECTRONIC BAND STRUCTURE

A. The empirical pseudopotential method

The EPM method[33] is employed for the calculation of the electronic band structure of the diamond cubic $Ge_{1-x}Sn_x$. The EPM is based on the orthogonalized plane wave (OPW)[34] method where the crystal wavefunction is constructed to be orthogonal to the core states. The pseudopotential Hamiltonian of semiconductors is given by

$$H = -\frac{\hbar^2}{2m}\nabla^2 + V_p(\boldsymbol{r}), \tag{1}$$

where V_p is the pseudopotential of the crystal that can be expanded into a Fourier series over the reciprocal lattice $\boldsymbol{G}$ as:

$$V_p(\boldsymbol{r}) = \sum_{\boldsymbol{G}} \left(V^S(\boldsymbol{G})S^S(\boldsymbol{G}) + iV^A(\boldsymbol{G})S^A(\boldsymbol{G})\right)e^{i\boldsymbol{G}.\boldsymbol{r}}. \tag{2}$$

In Eq. (2), $S^S(\boldsymbol{G})$ and $S^A(\boldsymbol{G})$ are the symmetric and asymmetric structural factors, respectively and $V^S(\boldsymbol{G})$ and $V^A(\boldsymbol{G})$ are the symmetric and asymmetric pseudopotential form factors, respectively. They are related to the cation atomic potential $V_1(\boldsymbol{G})$ and anion atomic potential $V_2(\boldsymbol{G})$ in the unit cell by

$$V^S(\boldsymbol{G}) = \frac{1}{2}[V_1(\boldsymbol{G}) + V_2(\boldsymbol{G})], \tag{3}$$

$$V^A(\boldsymbol{G}) = \frac{1}{2}[V_1(\boldsymbol{G}) - V_2(\boldsymbol{G})]. \tag{4}$$

The adjustment of the form factors corresponds to the selection of a good, though not unique, pseudopotential which can describe the material characteristics reasonably well. Since Ge and Sn both crystallize in the diamond structure, their asymmetric form factors are essentially zero $[V^A(G) = 0]$. Hence, it remains only the symmetric form factors for $Ge_{1-x}Sn_x$ alloys. The basic set of plane waves used in our EPM calculation were chosen such that $|\boldsymbol{G}+\boldsymbol{k}|$ lies within a sphere bounded by a kinetic energy E_1 with a magnitude of 13.5 Ry. By utilizing a perturbation method by Lowdin,[35] the second order contribution from all vectors $\boldsymbol{G}$ that satisfied the criterion of $E_1 < \frac{\hbar^2}{2m}|\boldsymbol{G}+\boldsymbol{k}|^2 < E_2$ with E_2 of 20.5 Ry was considered.[36]

Spin-orbit interaction is included for the accurate calculation of the band structures with the addition of the following spin-orbit matrix element:

$$H_{SO} = (\boldsymbol{K_i} \times \boldsymbol{K_j}).\sigma_{S,S'}[-i\lambda^S.S^S(\boldsymbol{G}) + \lambda^A.S^A(\boldsymbol{G})], \tag{5}$$

where $\boldsymbol{K_i} = \boldsymbol{G_i} + \boldsymbol{k}$, $\boldsymbol{K_j} = \boldsymbol{G_j} + \boldsymbol{k}$ and $\sigma_{S,S'}$ is the usual Pauli spin index denoting either spin up or down. λ^S and λ^A are the symmetric and asymmetric spin-orbit contributions, respectively. They are related the cationic and anionic spin-orbit contribution, λ_c and λ_a, by

$$\lambda^S = \frac{1}{2}(\lambda_c + \lambda_a), \quad \lambda^A = \frac{1}{2}(\lambda_c - \lambda_a), \tag{6}$$

where

$$\lambda_c = \mu B^c_{nl}(\boldsymbol{K}_i)B^c_{nl}(\boldsymbol{K}_j), \quad \lambda_a = \alpha\mu B^a_{nl}(\boldsymbol{K}_i)B^a_{nl}(\boldsymbol{K}_j). \tag{7}$$

μ is an adjustable spin-orbit parameter and α is the ratio of the spin splitting of the free anion and cation atoms. $B_{nl}(\boldsymbol{K})$ is defined by

$$B_{nl}(\boldsymbol{K}) = \beta\int_0^\infty j_{nl}(\boldsymbol{Kr})R_{nl}(\boldsymbol{r})r^2dr. \tag{8}$$

where β is a normalization constant. $j_{nl}(\boldsymbol{Kr})$ and $R_{nl}(\boldsymbol{r})$ are the spherical Bessel's function of lth angular momentum and the radial part of the core wavefunction, respectively.

B. EPM calculations

The VCA has been commonly used for the calculation of band structures of semiconductor alloys. In VCA, the semiconductor alloy consists of fictitious atoms each having an atomic potential being a compositionally weighted average of the atomic potentials of the constituent elemental atoms. Thus, VCA models alloys properties using atoms with mixed atomic potentials. VCA fails to describe correctly the characteristics of semiconductor alloys having band gap energies that vary strongly non-linearly with composition.[37] This inaccuracy arises from the nonlinear nature of composition dependence of atomic potential which is not well captured by VCA. Experimental work reported the direct band gap bowing parameter of $Ge_{1-x}Sn_x$ to be 1.94,[27] 2.1,[20] 2.3.[38] These large bowing parameters illustrate the nonlinear nature in which properties of $Ge_{1-x}Sn_x$ alloy depend on its composition.

In this study, the band structures of $Ge_{1-x}Sn_x$ alloys with different Sn compositions [0.05, 0.08, 0.11, 0.14, 0.17, and 0.20] were calculated using the EPM approach. The $Ge_{1-x}Sn_x$ alloy studied here is a random alloy with face-centered cubic (FCC) lattice, i.e., Sn atoms substitute for Ge atoms randomly throughout the crystal. The lattice constant $Ge_{1-x}Sn_x$ alloy was obtained by linear interpolation between the lattice constants of Ge and Sn atoms according to Vegard's rule.

Instead of using VCA in which the weighted potentials of the constituent atoms (Ge and Sn) are added to obtain the pseudopotential form factors, a set of pseudopotential form factors was adjusted for each Sn composition for the $Ge_{1-x}Sn_x$ alloy. The bowing parameters of direct and indirect band gap obtained by Costa *et al.*[27] were adopted in this work for the calculation of band gap energies at L and Γ-point at various Sn compositions. The band gap energies of Ref. 27 were used as benchmarks. For each Sn composition, the form factors were iteratively updated and fed into EPM until the calculated band structure of $Ge_{1-x}Sn_x$ yields band

gap energies which are in good agreement with the experimental values.

C. Results and discussions

The final adjusted form factors of $Ge_{1-x}Sn_x$ are summarized in Table I for Sn composition ranging from 5% to 20%. E_g^Γ and E_g^L are the band gap energies at the Γ and L-points, respectively. Overall, the fitted E_g^Γ and E_g^L agree well with experimentally reported band gap energies.[27] Using the fitted form factors, the electronic band structures of $Ge_{1-x}Sn_x$ along high symmetry lines in the Brillouin zone were calculated. The full electronic band structure of $Ge_{1-x}Sn_x$ with a Sn composition of 11% is plotted in Fig. 1. Fig. 2 shows the indirect to direct band gap transition for $Ge_{1-x}Sn_x$. For $x = 0.05$, the conduction band minimum (CBM) is located at L-point which is 0.573 eV above the valence band maximum (VBM) [Fig. 2(a)]. Fig. 2(b) shows that at $x = 0.11$, the band gap energies at the L and Γ-points are equal. Fig. 2(c) depicts the band structure of $Ge_{1-x}Sn_x$ with $x = 0.20$ which exhibits a direct band gap energy of 0.247 eV. The band gap energy of $Ge_{1-x}Sn_x$ at X (E_g^X), L (E_g^L), and Γ (E_g^Γ) points obtained from the band structures calculated by EPM is plotted against Sn compositions in Fig. 3. The E_g^Γ and E_g^L versus Sn composition curves from our calculations matched the corresponding curves of Ref. 27 which are plotted using dotted gray lines in Fig. 3.

From the calculated band structure of $Ge_{1-x}Sn_x$ alloy, the electron and hole effective masses along [100], [110], and [111] direction of the Brillouin zone were extracted using a simple parabolic line fit. All the extracted effective masses are in the unit of free electron mass, m_0. The heavy-hole (HH), light-hole (LH), split-off (SO), and conduction band effective masses of Germanium (Ge) (corresponding to $Ge_{1-x}Sn_x$ with Sn composition $x = 0.00$) extracted from our EPM calculation were compared to reported data in the literature in Tables II and III. The calculated effective masses in the conduction band (Table II) and in the valence band (Table III) for Ge agree well with reported data.

The HH and LH effective masses of $Ge_{1-x}Sn_x$ against Sn compositions are depicted in Figs. 4(a) and 4(b), respectively. From Fig. 4(a) a small variation (less than 7% with respect to HH effective mass of Ge) of HH effective mass with the Sn composition was noticed along [100], [110], and [111] directions. For all Sn compositions, HH effective mass is largest along [111] direction followed by [110] and [100] direction. Fig. 4(b) shows that LH effective mass decreases with progressively higher Sn composition along [100], [110], and [111] directions. LH along [111] has the smallest effective mass compared to that of [110] and [100] direction for the Sn compositions investigated. LH effective masses of different Sn composition were fitted with a quadratic polynomial. The fitted bowing equations for LH effective mass along [100], [110], and [111] directions are summarized in Table IV.

TABLE I. The fitted form factors for $Ge_{1-x}Sn_x$ with various Sn compositions used in EPM. The calculated band gap energies are in good agreement with the reported experimental data.[27] $V^S(3)$, $V^S(8)$, and $V^S(11)$ are the pseudopotential form factors for $\boldsymbol{G}^2$ equal to 3, 8, and 11 (in unit of $(2\pi/a)^2$ where a is the lattice constant).

				E_g^Γ		E_g^Γ	
x	$V^S(3)$	$V^S(8)$	$V^S(11)$	Expt. (Ref. 27)	This work	Expt. (Ref. 27)	This work
0.00	−0.27200	0.05700	0.01700	0.8000	0.8019	0.660	0.6581
0.05	−0.26972	0.05575	0.01516	0.6470	0.6478	0.573	0.5727
0.08	−0.26825	0.05495	0.01418	0.5602	0.5605	0.524	0.5240
0.11	−0.26600	0.05345	0.01380	0.4766	0.4771	0.477	0.4769
0.14	−0.26410	0.05220	0.01330	0.3966	0.3966	0.432	0.4330
0.17	−0.26315	0.05190	0.01210	0.3201	0.3183	0.390	0.3900
0.20	−0.26130	0.05084	0.01160	0.2470	0.2475	0.350	0.3505

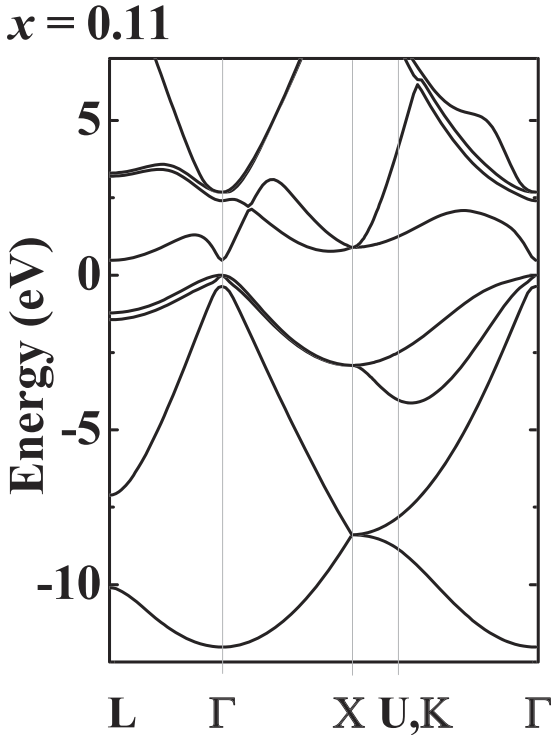

FIG. 1. Full band structure of $Ge_{1-x}Sn_x$ along high symmetry lines in the Brillouin zone for $x = 0.11$. The Brillouin zone of the $Ge_{1-x}Sn_x$ alloy is similar to that of face-centered cubic (FCC) Ge.

Fig. 5(a) shows the transverse $m_{e,t}^{*L}$ and longitudinal $m_{e,l}^{*L}$ electron effective masses at L-point. The effect of varying Sn composition in $Ge_{1-x}Sn_x$ is almost negligible for the longitudinal electron effective mass $m_{e,l}^{*L}$. The variation of $m_{e,l}^{*L}$ of $Ge_{1-x}Sn_x$ with respect to $m_{e,l}^{*L}$ of Ge is less than 1.5%. For transverse electron effective mass $m_{e,t}^{*L}$, it shows a nearly linear reduction trend with increasing Sn composition. The electron effective mass at Γ-point $m_e^{*\Gamma}$ is shown in Fig. 5(b). By raising Sn composition in $Ge_{1-x}Sn_x$ from $x = 0$ to $x = 0.2$, $m_e^{*\Gamma}$ is reduced noticeably by about 60%. The bowing equation for the electron effective masses is deduced and summarized in Table IV.

The band structures for bulk $Ge_{1-x}Sn_x$ alloys were calculated in order to investigate the dependence of effective masses of bulk $Ge_{1-x}Sn_x$ alloys along different crystal directions on each crystal plane orientation. It should be noted that we are referring to band structures of bulk $Ge_{1-x}Sn_x$ and not of $Ge_{1-x}Sn_x$ crystal surfaces. Three common plane

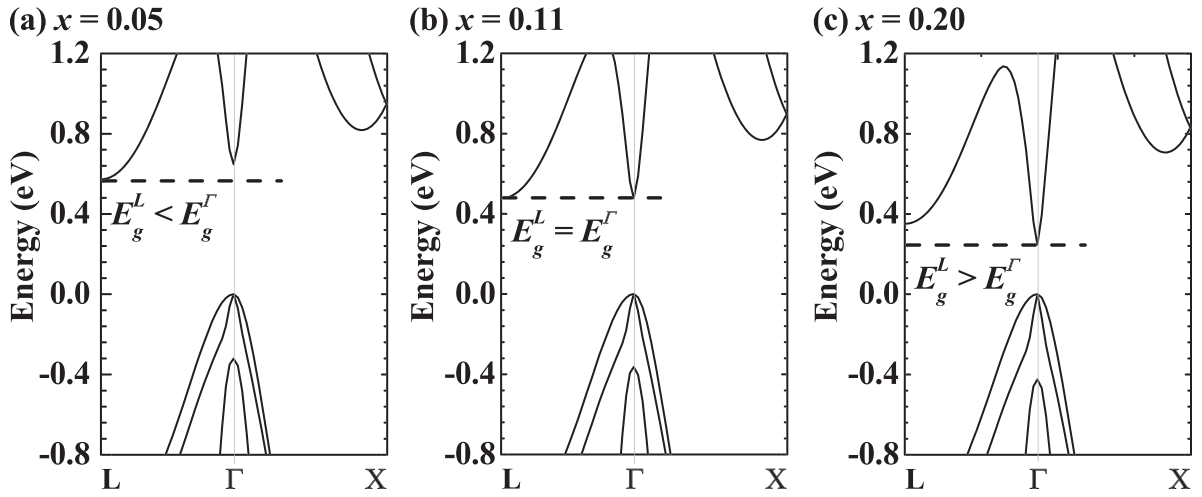

FIG. 2. Zoomed-in view of the electronic band structures of $Ge_{1-x}Sn_x$ along L-Γ-X for (a) $x = 0.05$, (b) $x = 0.11$, and (c) $x = 0.20$, showing the transition from indirect [Fig. 2(a)] to direct band gap [Fig. 2(c)]. Fig. 2(b) illustrates the critical composition of 11% where the band gap energies at the L and Γ-points are equal.

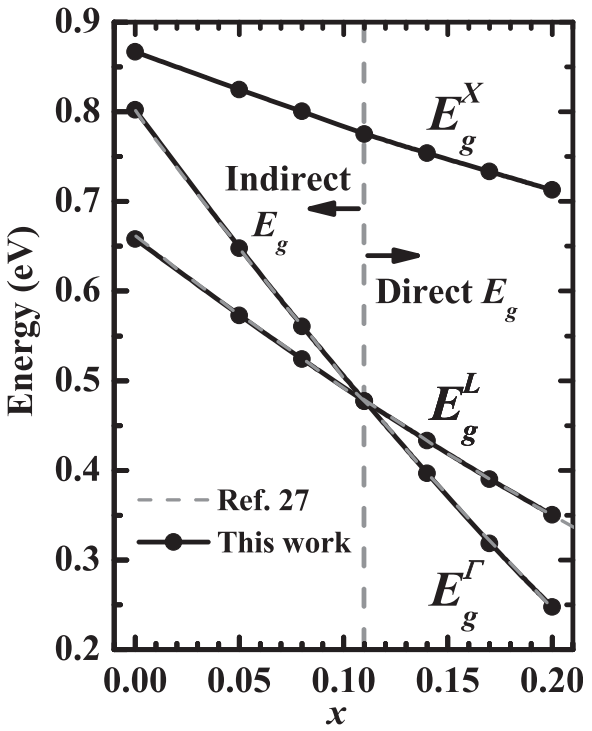

FIG. 3. The calculated band gap energies of X, L, and Γ-point at various Sn compositions. The band gap energies of L and Γ-point agree well with the experimentally reported values in Ref. 27.

TABLE II. Effective masses of conduction band at symmetry points (L, Γ, and Δ) in the Brillouin zone.

	(m_0 unit)	$m_{e,l}^{*L}$	$m_{e,t}^{*L}$	$m_e^{*\Gamma}$	$m_{e,l}^{*\Delta}$	$m_{e,t}^{*\Delta}$
Ge	This work	1.595	0.092	0.0420	0.952	0.206
	Literature	1.578[a]	0.093[a]	0.0470[a]	0.889[a]	0.194[a]
		1.610[b]	0.081[b]	0.0380[b]	1.350[b]	0.290[b]
		1.568[c]	0.094[c]	0.0490[c]	1.851[c]	0.195[c]

[a]Ref. 39.
[b]Ref. 40.
[c]Ref. 41.

orientations of (100), (110), and (111) were studied. For each plane orientation, the effective masses along all in-plane directions were considered. Figs. 6–8 portray the effect of plane orientation and in-plane directions on electron and hole effective masses at Γ-point. The inset of Fig. 6 shows the top views of wafers with (100), (110), and (111) planes. For each plane, various in-plane directions within the horizontal and vertical axes (from 0° to 90°) were considered. For (100) plane, 0° and 90° correspond to [001] and [010] directions, respectively. For (110) plane, 0° and 90° were taken along [001] and [1$\bar{1}$0] directions. For (111) plane, the corresponding directions for 0° and 90° are [$\bar{1}$10] and [$\bar{1}\bar{1}$2], respectively.

From Figs. 6(a) and 6(b), the LH effective mass of (100) and (110) plane orientations shows slight anisotropy. For (100) plane orientation, the LH effective mass decreases with increasing in-plane direction from 0° to 50° while it starts to increase from 50° to 90° [Fig. 6(a)]. Fig. 6(b) shows the trend of decreased LH effective mass with increasing in-plane directions from 0° to 90° for (110) plane orientation. Fig. 6(c) illustrates that the LH effective mass of (111) plane is isotropic with all the in-plane directions having a similar effective mass.

For the HH effective mass, an evident anisotropy was observed for (100) and (110) plane orientations. For (100) plane orientation, HH effective mass increases from 0° to

TABLE III. Effective masses of heavy-hole, light-hole and split-off bands along symmetry lines [(100), (110), and (111)] in the Brillouin zone.

		$m_{hh}^{*\Gamma}$			$m_{lh}^{*\Gamma}$			
	(m_0 unit)	(100)	(110)	(111)	(100)	(110)	(111)	m_{so}
Ge	This work	0.226	0.439	0.597	0.0529	0.0476	0.0463	0.116
	Literature	0.251[a]	0.467[a]	0.623[a]	0.0600[a]	0.0530[a]	0.0520[a]	0.128[a]
		0.254[b]	0.477[b]	0.390[b]	0.0490[b]	0.0560[b]	0.0550[b]	0.097[c]

[a]Ref. 39.
[b]Ref. 41.
[c]Ref. 42.

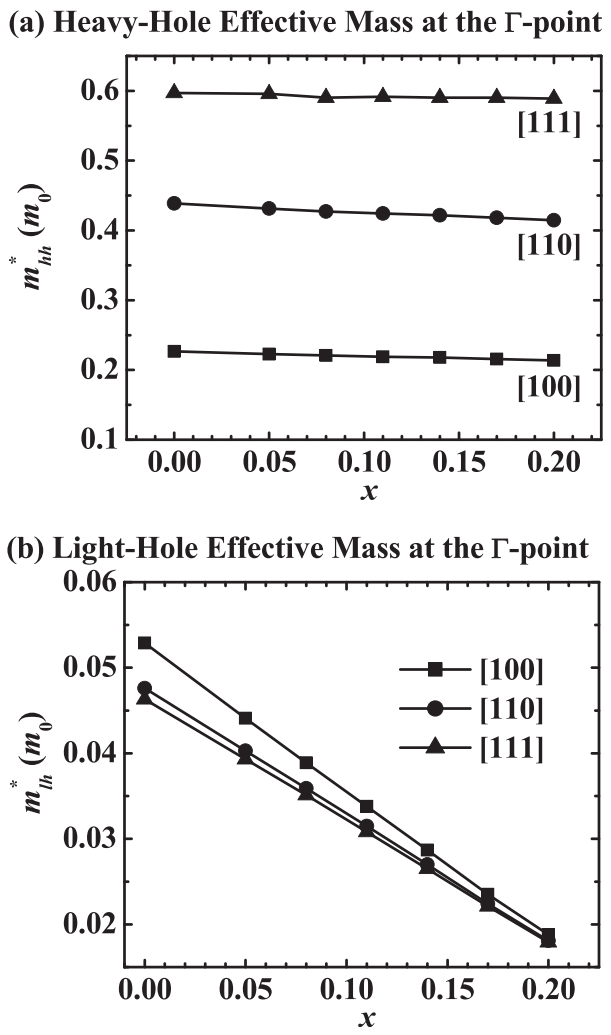

FIG. 4. (a) Heavy-hole (HH) and (b) light-hole (LH) effective masses of $Ge_{1-x}Sn_x$ along high symmetry lines in the Brillouin zone for x ranging from 0.05 to 0.20.

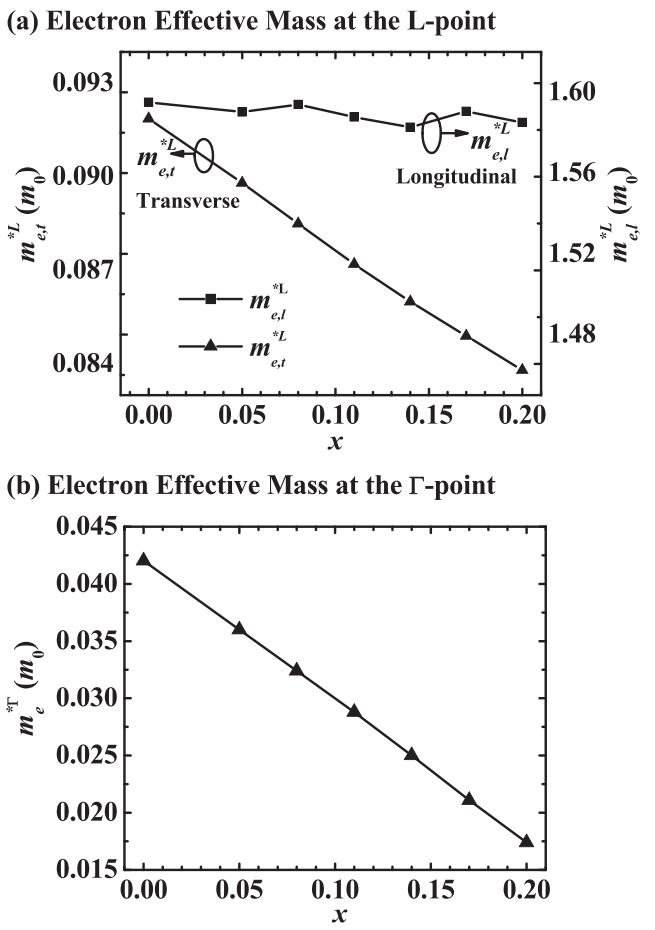

FIG. 5. Electron effective masses of $Ge_{1-x}Sn_x$ along high symmetry lines in the Brillouin zone for x ranging from 0.05 to 0.20: (a) Longitudinal and transverse electron effective mass at L-point, (b) Electron effective mass at Γ-point.

45° and decreases from 45° to 90° shown in Fig. 7(a). From Fig. 7(b), HH effective mass shows a similar trend as that of (100) plane orientation with increasing effective mass from 0° to 60° and decreasing from 60° to 90°. The HH of (111) plane orientation is rather isotropic for all in-plane directions shown in Fig. 7(c). The reduction of the HH effective mass with increasing Sn composition for three planes and all plane orientations is much less pronounced compared to the reduction seen in the LH effective mass.

For electron effective mass at Γ-point, it appears to be independent of the in-plane directions for all (100), (110), and (111) plane orientations shown in Figs. 8(a)–8(c). Three plane orientations demonstrate a similar trend of electron effective mass along all in-plane directions.

Overall, the effective masses of LH, HH, and conduction band at Γ-point along all in-plane directions decrease with the increasing of Sn composition for all three plane orientations. This observation is consistent with the fact of reduced band gap energy of $Ge_{1-x}Sn_x$ alloy with increasing Sn composition which leads to smaller effective masses for $Ge_{1-x}Sn_x$ alloy with higher Sn composition.

TABLE IV. The bowing equations for light-hole, heavy-hole, and electron effective masses (in unit of m_0) fitted with a quadratic polynomial for $0 \le x \le 0.20$.

Effective mass	Bowing equation (least squares fit)
m_{lh} [100]	$0.03669x^2 - 0.1781x + 0.05288$
m_{lh} [110]	$-0.01199x^2 - 0.1456x + 0.04759$
m_{lh} [111]	$-0.01992x^2 - 0.1384x + 0.04628$
m_e [111]	$0.009216x^2 - 0.1299x + 0.04202$

III. DERIVATION OF EFFECTIVE MASS PARAMETERS

A. Effective mass approximation

k.p method has been commonly used for obtaining the electronic band structures of semiconductor materials for device designs, such as carrier mobility[43] and optical gain of quantum well laser.[44] The extraction of k.p effective mass parameters can be obtained by fitting the electronic band structures of k.p method to that of EPM.[36,45,46] Using 8-band k.p Hamiltonian,[47] the band edge dispersion at the Γ-point obtained by k.p method was fitted to the EPM results by tuning the adjustable Luttinger-like parameters. The 8-band Hamiltonian for a diamond structure is given as

$$H = \begin{bmatrix} C & 0 & \frac{1}{\sqrt{2}}P_- & -\sqrt{\frac{2}{3}}P_Z & -\frac{1}{\sqrt{6}}P_+ & 0 & -\frac{1}{\sqrt{3}}P_Z & -\frac{1}{\sqrt{3}}P_+ \\ 0 & C & 0 & \frac{1}{\sqrt{6}}P_- & -\sqrt{\frac{2}{3}}P_Z & -\frac{1}{\sqrt{2}}P_+ & -\frac{1}{\sqrt{3}}P_- & \frac{1}{\sqrt{3}}P_Z \\ \frac{1}{\sqrt{2}}P_- & 0 & HH & S & -R & 0 & \frac{S}{\sqrt{2}} & -\sqrt{2}R \\ -\sqrt{\frac{2}{3}}P_Z & \frac{1}{\sqrt{6}}P_- & S^* & LH & 0 & -R & -D & -\sqrt{\frac{2}{3}}S \\ -\frac{1}{\sqrt{6}}P_+ & -\sqrt{\frac{2}{3}}P_Z & -R^* & 0 & LH & -S & -\sqrt{\frac{2}{3}}S^* & D \\ 0 & -\frac{1}{\sqrt{2}}P_+ & 0 & -R^* & -S^* & HH & \sqrt{2}R^* & \frac{S^*}{\sqrt{2}} \\ -\frac{1}{\sqrt{3}}P_Z & -\frac{1}{\sqrt{3}}P_- & \frac{S^*}{\sqrt{2}} & -D & -\sqrt{\frac{2}{3}}S & \sqrt{2}R & V & 0 \\ -\frac{1}{\sqrt{3}}P_+ & \frac{1}{\sqrt{3}}P_Z & -\sqrt{2}R^* & -\sqrt{\frac{2}{3}}S^* & D & \frac{S}{\sqrt{2}} & 0 & V \end{bmatrix}, \quad (9)$$

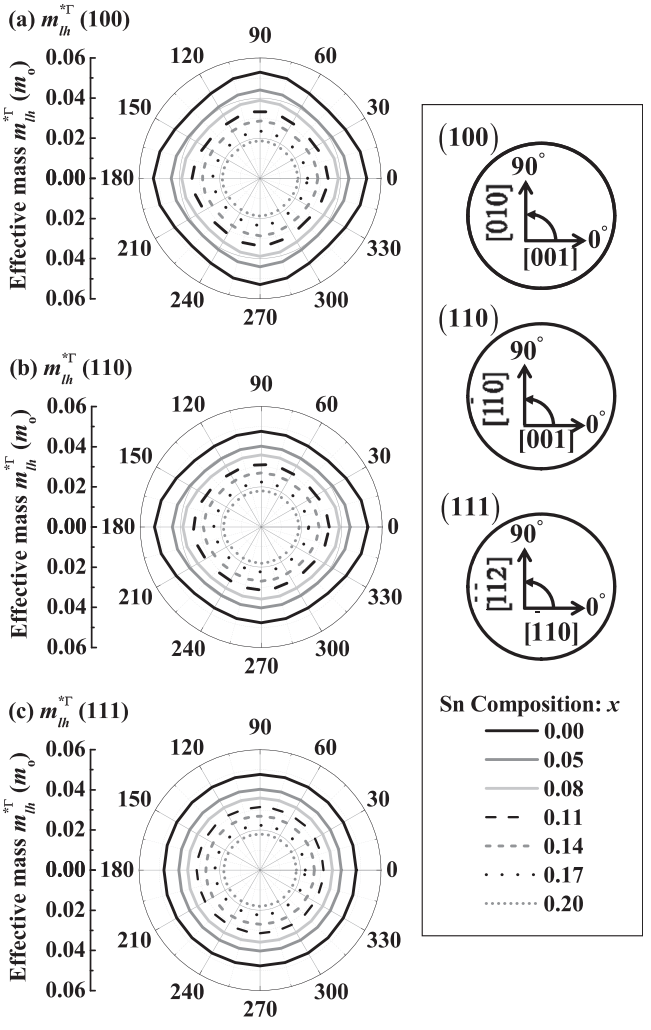

FIG. 6. The effective masses for light-hole, heavy-hole, and conduction band at Γ-point of $Ge_{1-x}Sn_x$ for three common plane orientations [(100), (110), and (111)] and various in-plane directions. The LH effective masses along various in-plane directions for different plane orientations: (a) (100), (b) (110), and (c) (111). The LH effective mass of (100) and (110) shows slight anisotropy.

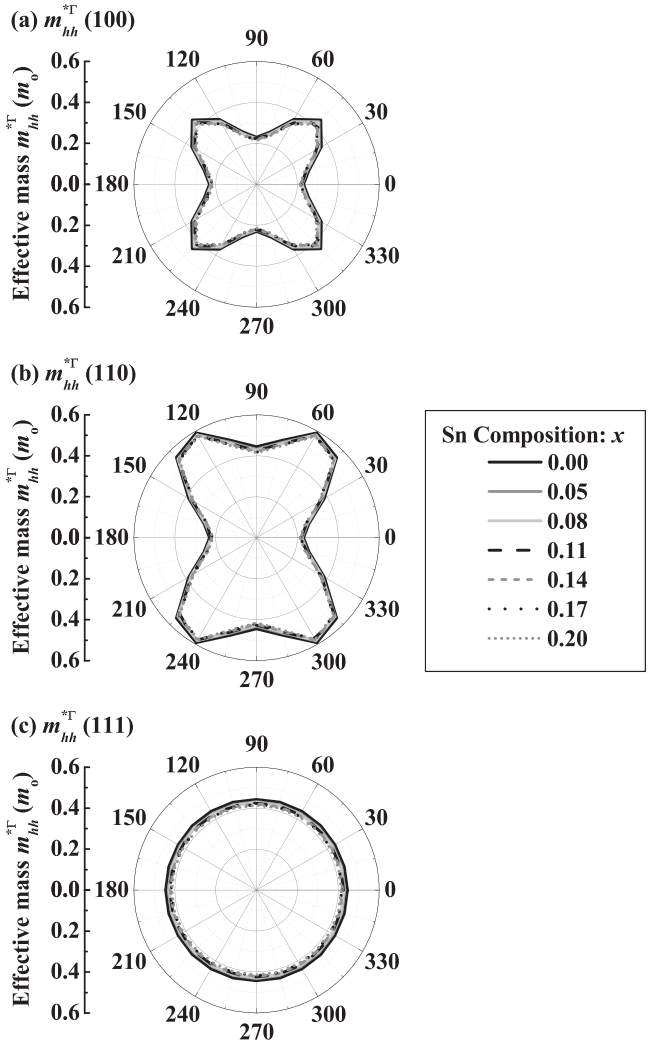

FIG. 7. The effective masses of HH for three plane orientations: (a) (100), (b) (110), and (c) (111). The effective masses for (100) and (110) plane orientations show evident anisotropy.

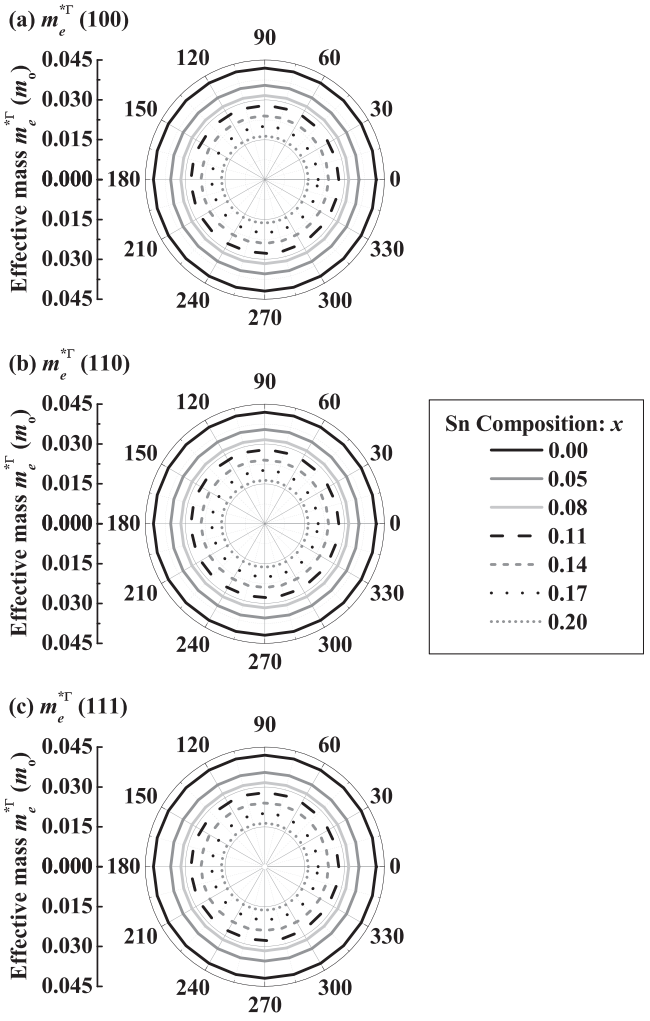

FIG. 8. The effective masses of electron for three plane orientations: (a) (100), (b) (110), and (c) (111). The effective masses for all plane orientations are isotropic for all the in-plane directions.

where

$$C = E_g^{\Gamma} + \frac{\hbar^2}{2m_0}\left(\frac{1}{m_c} - \frac{E_p}{3}\left[\frac{2}{E_g^{\Gamma}} + \frac{1}{E_g^{\Gamma}+\Delta}\right]\right)(k_x^2 + k_y^2 + k_z^2), \tag{10a}$$

$$HH = -\frac{\hbar^2}{2m_0}[(\gamma_1+\gamma_2)(k_x^2+k_y^2) + (\gamma_1 - 2\gamma_2)k_z^2], \tag{10b}$$

$$LH = -\frac{\hbar^2}{2m_0}[(\gamma_1-\gamma_2)(k_x^2+k_y^2) + (\gamma_1 + 2\gamma_2)k_z^2], \tag{10c}$$

$$V = -\frac{\hbar^2}{2m_0}\gamma_1(k_x^2+k_y^2+k_z^2) - \Delta, \tag{10d}$$

$$S = -\frac{\hbar^2}{2m_0}2\sqrt{3}\gamma_3(-k_x + ik_y)k_z, \tag{10e}$$

$$R = -\frac{\hbar^2}{2m_0}\sqrt{3}[\gamma_2(k_x^2 - k_y^2) - 2\gamma_3 i k_x k_y], \tag{10f}$$

$$D = -\frac{\hbar^2}{2m_0}\sqrt{2}\gamma_2(k_x^2 + k_y^2 - 2k_z^2), \tag{10g}$$

$$P_{\pm} = P_o(k_x \pm ik_y), \tag{10h}$$

$$P_z = P_o k_z. \tag{10i}$$

m_c is the electron effective mass. Δ accounts for the spin-orbit interaction. γ_1, γ_2, and γ_3 are the modified effective mass parameters and related to the Luttinger parameters (γ_1^L,γ_2^L,γ_3^L) used in 6-band Hamiltonian by[48]

$$\gamma_1 = \gamma_1^L - \frac{E_p}{3E_g}, \quad \gamma_2 = \gamma_2^L - \frac{E_p}{6E_g}, \quad \gamma_3 = \gamma_3^L - \frac{E_p}{6E_g}. \tag{11}$$

The mixing of the valence and conduction bands is governed by Kane energy E_p and it is related to P_o by

$$E_p = \frac{2m_0}{\hbar^2}P_0{}^2. \tag{12}$$

In addition, the Luttinger parameters are approximately related to the heavy-hole and light-hole effective masses[49] by

$$\gamma_1^L = \frac{1}{2}\left(\frac{1}{m_{lh}^{[001]}} + \frac{1}{m_{hh}^{[001]}}\right),$$
$$\gamma_2^L = \frac{1}{4}\left(\frac{1}{m_{lh}^{[001]}} - \frac{1}{m_{hh}^{[001]}}\right),$$
$$\gamma_3^L = \frac{1}{4}\left(\frac{1}{m_{lh}^{[001]}} + \frac{1}{m_{hh}^{[001]}}\right) - \frac{1}{2m_{hh}^{[111]}}. \tag{13}$$

where $m_{hh(lh)}^{[001]}$ and $m_{hh(lh)}^{[111]}$ are heavy-hole (light-hole) effective mass in [001] and [111] directions, respectively. Once the 8-band k.p Hamiltonian is established, the energy dispersion in the vicinity of the Γ-point can be obtained by diagonalizing the Hamiltonian matrix.

B. Discussions and results of numerical fitting

Since the band gap of $Ge_{1-x}Sn_x$ alloy at Γ-point reduces with increasing Sn composition, the coupling of conduction band with valence band needs to be included for accurate calculations of band structures. Thus, 8-band k.p Hamiltonian was chosen over 6-band k.p Hamiltonian in order to account for the coupling between conduction and valence bands. The Luttinger-like parameters, γ_1, γ_2, and γ_3, are treated as adjustable parameters. Vegard′s law was used to approximate other required parameters, such as Kane energy and lattice constant for each Sn composition of $Ge_{1-x}Sn_x$. Since the energy dispersion in the small vicinity of the Γ-point determines the transport behavior of semiconductors, accurate energy dispersion at the band edge is crucial. Hence, the fitting of band structure by k.p method to ones by EPM is aimed at reproducing effective masses obtained from band structures by EPM.

For the fitting process, the initial guesses of the fitting parameters were calculated by Eq. (13) based on the electron and hole effective masses at Γ-point obtained by EPM. For each fitting iteration, the effective masses of HH, LH, split-off (SO), and conduction bands (CB) were extracted from

TABLE V. The fitted Luttinger-like parameters, including Kane energy E_p, band gap energy at the Γ-point E_g^Γ, and spin-orbit splitting Δ for $0 \le x \le 0.20$.

x	γ_1	γ_2	γ_3	E_p	E_g^Γ	Δ
0.05	13.6487	4.5823	5.9854	26.185	0.6478	0.3209
0.08	15.2093	5.3417	6.7572	26.116	0.5605	0.3423
0.11	17.2307	6.3319	7.7708	26.047	0.4771	0.3635
0.14	19.9506	7.6821	9.1278	25.978	0.3966	0.3845
0.17	23.8490	9.5988	11.0770	25.909	0.3182	0.4048
0.20	29.5552	12.4408	13.9287	25.840	0.2475	0.4249

TABLE VI. The effective masses of the LH and HH bands of $Ge_{1-x}Sn_x$ (in unit of m_0) obtained using a simple parabolic line fit using 8-band k.p method and EPM for $0 \le x \le 0.20$.

	m_{lh} (k.p, EPM)		m_{hh} (k.p, EPM)	
x	[100]	[111]	[100]	[111]
0.05	0.0529, 0.0529	0.0464, 0.0464	0.230, 0.230	0.604, 0.603
0.08	0.0441, 0.0441	0.0393, 0.0393	0.223, 0.223	0.596, 0.596
0.11	0.0389, 0.0389	0.0351, 0.0351	0.221, 0.221	0.590, 0.590
0.14	0.0338, 0.0338	0.0308, 0.0308	0.219, 0.219	0.592, 0.592
0.17	0.0287, 0.0287	0.0265, 0.0265	0.218, 0.218	0.590, 0.590
0.20	0.0235, 0.0235	0.0221, 0.0221	0.215, 0.215	0.590, 0.590

the band structures calculated by k.p method. These extracted effective masses were then compared with that of EPM. In the fitting process, the fitting parameters were iteratively adjusted in order to minimize the difference between effective masses obtained by k.p method and EPM.

TABLE VII. The effective masses of the conduction and split-orbit bands of $Ge_{1-x}Sn_x$ (in unit of m_0) obtained using a simple parabolic line fit using 8-band k.p method and EPM for $0 \le x \le 0.20$.

	m_e (k.p, EPM)		m_{so} (k.p, EPM)	
x	[100]	[111]	[100]	[111]
0.05	0.0355, 0.0355	0.0356, 0.0355	0.109, 0.109	0.108, 0.108
0.08	0.0316, 0.0316	0.0317, 0.0317	0.107, 0.104	0.107, 0.104
0.11	0.0278, 0.0278	0.0278, 0.0279	0.107, 0.100	0.106, 0.100
0.14	0.0240, 0.0240	0.0240, 0.0240	0.108, 0.096	0.108, 0.0958
0.17	0.0201, 0.0201	0.0202, 0.0201	0.114, 0.0915	0.114, 0.0913
0.20	0.0164, 0.0164	0.0165, 0.0164	0.132, 0.0875	0.131, 0.0874

The fitted Luttinger parameters of 8-band k.p method for each Sn composition of $Ge_{1-x}Sn_x$ are summarized in Table V. The comparison of the effective masses of HH, LH, SO, and CB at different Sn composition obtained by k.p method and EPM is shown in Tables VI and VII. In Fig. 9, the band structures of $Ge_{1-x}Sn_x$ alloy by k.p method are compared to that of EPM for $x = 0.05$, 0.11, and 0.20. The band structures obtained by k.p method (dashed line) were fitted reasonably well to that by EPM which is plotted with open circles.

For Sn composition x from 0.05 to 0.20, the average difference between HH, LH, and CB effective masses obtained by k.p and by EPM is within 0.08%, indicating that a very good fitting was achieved. The average discrepancy for SO effective mass calculated by k.p method and by EPM is

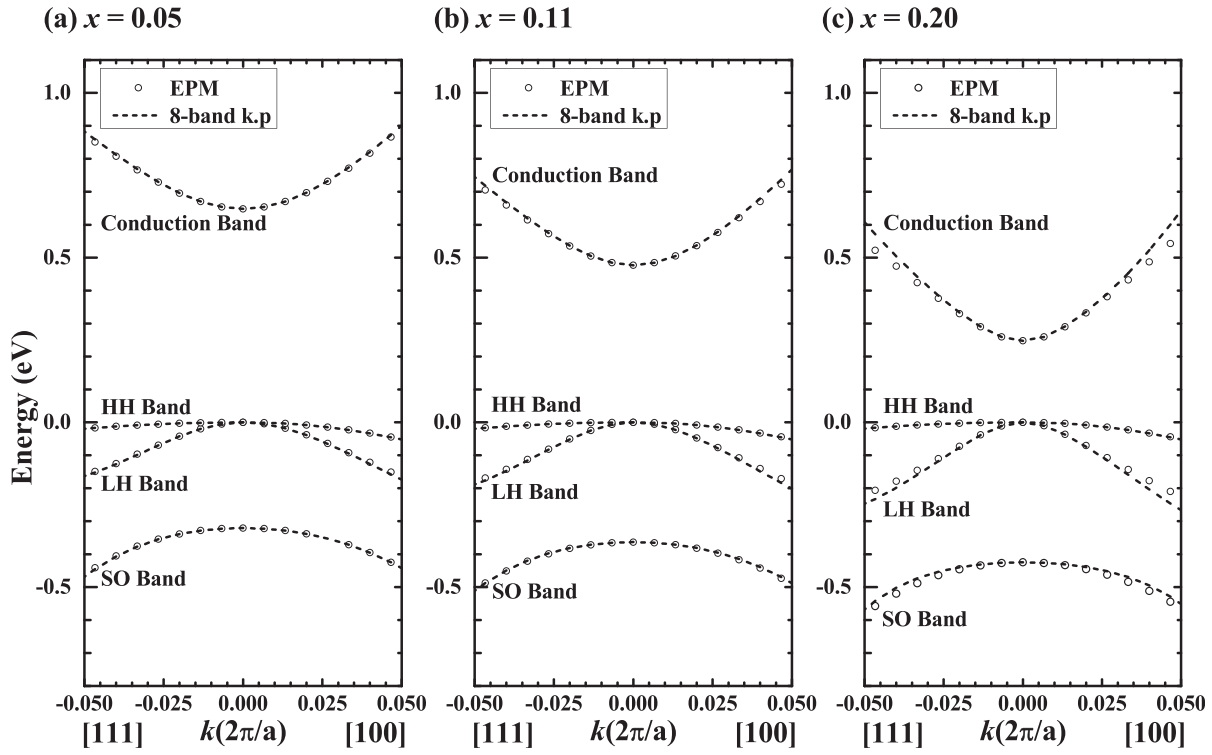

FIG. 9. The fitted band structures of $Ge_{1-x}Sn_x$ for (a) $x = 0.05$, (b) $x = 0.11$, and (c) $x = 0.20$ at Γ-point using 8-band k.p Hamiltonian with the spin-orbit interaction taken into account. The results of EPM calculation are plotted with open circles, and results from the k.p method are plotted using dashed lines.

about 19%. Since the transport of semiconductors is essentially determined by HH, LH, and CB effective masses, the effect of SO effective mass is generally negligible. So, an average difference of 18% difference in SO effective mass will not affect the transport behavior of $Ge_{1-x}Sn_x$ alloys. Overall, from the results of Tables VI, VII, and Fig. 9, the 8-band k.p method successfully reproduces the energy dispersions calculated by EPM at the vicinity of Γ- point.

IV. CONCLUSION

The electronic band structures of $Ge_{1-x}Sn_x$ were calculated using the empirical pseudopotential method. By adjusting the form factors of the pseudopotential, the band gap energies obtained from the calculated band structures agree well with reported experimental data. With increasing Sn composition, the extracted $Ge_{1-x}Sn_x$ effective masses decrease for $0 < x < 0.20$ for light-hole valence band, conduction band at Γ-point and conduction band at L-point along transverse direction. The effective masses of heavy-hole and conduction band at L-point along longitudinal direction are rather independent of Sn composition. The study of the dependence of effective masses at Γ-point on the plane orientations [(001), (110) and (111)] and in-plane directions reveals that the LH and HH effective masses show anisotropy for plane orientations of (100) and (110). For electron effective mass, it shows isotropy and similar magnitude along all in-plane directions for all three plane orientations investigated. In addition, the Luttinger-like parameters of 8-band k.p model were derived by fitting the energy dispersion in the vicinity of the Γ-point to that by EPM. These effective masses and derived effective mass parameters of 8-band k.p method may be useful for the optical and electronic device designs employing $Ge_{1-x}Sn_x$ alloys.

ACKNOWLEDGMENTS

Research grant from the Singapore National Research Foundation (NRF) (NRF-RF2008-09) and Graduate Research Scholarship are acknowledged.

[1]Y. Chibane, B. Bouhafs, and M. Ferhat, Phys. Status Solidi B **240**, 116 (2003).
[2]W.-J. Yin, X.-G. Gong, and S.-H. Wei, Phys. Rev. B **78**, 161203 (2008).
[3]P. Moontragoon, Z. Ikonić, and P. Harrison, Semicond. Sci. Technol. **22**, 742 (2007).
[4]Y. Chibane and M. Ferhat, J. Appl. Phys. **107**, 053512 (2010).
[5]N. Bouarissa and F. Annane, Mater. Sci. Eng., B **95**, 100 (2002).
[6]B. Bouhafs, F. Benkabou, M. Ferhat, B. Khelifa, J. P. Dufour, and H. Aourag, Infrared Phys. Technol. **36**, 967 (1995).
[7]K. A. Mäder, A. Baldereschi, and H. von Känel, Solid State Commun. **69**, 1123 (1989).
[8]D. W. Jenkins and J. D. Dow, Phys. Rev. B **36**, 7994 (1987).
[9]P. R. Pukite, A. Harwit, and S. S. Iyer, Appl. Phys. Lett. **54**, 2142, (1989).
[10]M. T. Asom, E. A. Fitzgerald, A. R. Kortan, B. Spear, and L. C. Kimerling, Appl. Phys. Lett. **55**, 578 (1989).
[11]H. Höchst, M. A. Engelhardt, and I. Hernández-Calderón, Phys. Rev. B **40**, 9703 (1989).
[12]J. R. C. Bowman, P. M. Adams, M. A. Engelhardt, and H. Höchst, J. Vac. Sci. Technol. A **8**, 1577 (1990).
[13]J. Piao, R. Beresford, T. Licata, W. I. Wang, and H. Homma, J. Vac. Sci. Technol. B **8**, 221 (1990).
[14]O. Gurdal, M.-A. Hasan, J. M. R. Sardela, J. E. Greene, H. H. Radamson, J. E. Sundgren, and G. V. Hansson, Appl. Phys. Lett. **67**, 956 (1995).
[15]G. He and H. A. Atwater, Phys. Rev. Lett. **79**, 1937 (1997).
[16]M. E. Taylor, G. He, H. A. Atwater, and A. Polman, J. Appl. Phys. **80**, 4384 (1996).
[17]O. Gurdal, P. Desjardins, J. R. A. Carlsson, N. Taylor, H. H. Radamson, J.-E. Sundgren, and J. E. Greene, J. Appl. Phys. **83**, 162 (1998).
[18]R. Ragan and H. A. Atwater, Appl. Phys. Lett. **77**, 3418 (2000).
[19]H. Lin, R. Chen, Y. Huo, T. I. Kamins, and J. S. Harris, Appl. Phys. Lett. **98**, 261917 (2011).
[20]R. Chen, H. Lin, Y. Huo, C. Hitzman, T. I. Kamins, and J. S. Harris, Appl. Phys. Lett. **99**, 181125 (2011).
[21]H. Lin, R. Chen, W. Lu, Y. Huo, T. I. Kamins, and J. S. Harris, Appl. Phys. Lett. **100**, 102109 (2012).
[22]J. Taraci, J. Tolle, J. Kouvetakis, M. R. McCartney, D. J. Smith, J. Menendez, and M. A. Santana, Appl. Phys. Lett. **78**, 3607 (2001).
[23]M. Bauer, J. Taraci, J. Tolle, A. V. G. Chizmeshya, S. Zollner, D. J. Smith, J. Menendez, C. Hu, and J. Kouvetakis, Appl. Phys. Lett. **81**, 2992 (2002).
[24]M. R. Bauer and J. Tolle, Solid State Commun. **127**, 355 (2003).
[25]M. R. Bauer, C. S. Cook, P. Aella, J. Tolle, J. Kouvetakis, P. A. Crozier, A. V. G. Chizmeshya, D. J. Smith, and S. Zollner, Appl. Phys. Lett. **83**, 3489 (2003).
[26]P. Aella, C. Cook, J. Tolle, S. Zollner, A. V. G. Chizmeshya, and J. Kouvetakis, Appl. Phys. Lett. **84**, 888 (2004).
[27]V. R. D'Costa, C. S. Cook, A. G. Birdwell, C. L. Littler, M. Canonico, S. Zollner, J. Kouvetakis, and J. Menéndez, Phys. Rev. B **73**, 125207 (2006).
[28]S. Oguz, W. Paul, T. F. Deutsch, B.-Y. Tsaur, and D. V. Murphy, Appl. Phys. Lett. **43**, 848 (1983).
[29]S. I. Shah, J. E. Greene, L. L. Abels, Q. Yao, and P. M. Raccah, J. Cryst. Growth **83**, 3 (1987).
[30]S. M. Lee, J. Appl. Phys. **75**, 1987 (1994).
[31]H. Pérez Ladrón De Guevara, A. G. Rodríguez, H. Navarro-Contreras, and M. A. Vidal, Appl. Phys. Lett. **83**, 4942 (2003).
[32]H. Pérez Ladrón de Guevara, A. G. Rodríguez, H. Navarro-Contreras, and M. A. Vidal, Appl. Phys. Lett. **84**, 4532 (2004).
[33]M. L. Cohen and T. K. Bergstresser, Phys. Rev. **141**, 789 (1966).
[34]C. Herring, Phys. Rev. **57**, 1169 (1940).
[35]P. Löwdin, J. Chem. Phys. **19**, 1396 (1951).
[36]Y.-C. Yeo, T. C. Chong, and M. F. Li, J. Appl. Phys. **83**, 1429 (1998).
[37]M. Jaros, Rep. Prog. Phys. **48**, 1091 (1985).
[38]H. Pérez Ladrón de Guevara, A. G. Rodríguez, H. Navarro-Contreras, and M. A. Vidal, Appl. Phys. Lett. **91**, 161909 (2007).
[39]J. Kim and M. V. Fischetti, J. Appl. Phys. **108**, 013710 (2010).
[40]S. Adachi, *Properties of Semiconductor Alloys: Group-IV, III-V and II-VI Semiconductors* (Wiley, New York, 2009).
[41]M. Fischetti and J. Higman, *in Monte Carlo Device Simulation: Full Band and Beyond*, edited by K. Hess (Kluwer Academic, Norwell, 1991), Chap. 5, pp. 123–160.
[42]*Landolt-Bornstein: Numerical Data and Functional Relationships in Science and Technology*, edited by O. Madelung, New Series Group III Vol. 17C (Springer, Berlin, 1982).
[43]M. V. Fischetti, Z. Ren, P. M. Solomon, M. Yang, and K. Rim, J. Appl. Phys. **94**, 1079 (2003).
[44]Y.-H. Zhu, Q. Xu, W.-J. Fan, and J.-W. Wang, J. Appl. Phys. **107**, 073108 (2010).
[45]P. Moontragoon, N. Vukmirović, Z. Ikonić, and P. Harrison, J. Appl. Phys. **103**, 103712, (2008).
[46]W. J. Fan, A. P. Abiyasa, S. T. Tan, S. F. Yu, X. W. Sun, J. B. Xia, Y.-C. Yeo, M. F. Li, and T. C. Chong, J. Crystal Growth **287**, 28, (2006).
[47]S. Ridene, K. Boujdaria, H. Bouchriha, and G. Fishman, Phys. Rev. B **64**, 085329 (2001).
[48]C. R. Pidgeon and R. N. Brown, Phys. Rev. **146**, 575 (1966).
[49]T. E. Ostromek, Phys. Rev. B **54**, 14467 (1996).